

*Electronic Supplementary Information (ESI) for*

## **Dynamic Wrinkling of Hydrogel-Elastomer Hybrid Microtube Enables Blood Vessel-like Hydraulic Pressure Sensing and Flow Regulation**

Xuelian Wen, Shengtong Sun\*, and Peiyi Wu\*

E-mail: [shengtongsun@dhu.edu.cn](mailto:shengtongsun@dhu.edu.cn); [wupeiyi@dhu.edu.cn](mailto:wupeiyi@dhu.edu.cn)

### **This material includes**

#### **Experimental**

- Fig. S1** Schematic fabrication process of PCMH@TPE microtube
- Fig. S2** XRD profiles of raw  $\text{Ti}_3\text{AlC}_2$  and exfoliated 2D MXene ( $\text{Ti}_3\text{C}_2\text{T}_x$ ) nanosheets
- Fig. S3** Typical (a) TEM and (b) AFM images of MXene nanosheets
- Fig. S4** Cross-sectional images of a single microtube at different positions and multiple microtubes
- Fig. S5** DSC heating curves of PNIPAM/clay hydrogel and PCMH
- Fig. S6** Heat-induced channel size changes of PCMH@TPE microtubes with elliptical and square cross-sections
- Fig. S7** Optical images of PCMH peeled from TPE tube pre-treated with benzophenone
- Fig. S8** ATR-FTIR spectra of 4-ABP, 4-ABP treated TPE and pure TPE
- Fig. S9** Schematic interfacial bonding between PCMH and TPE with the strategy of 4-ABP pre-treatment
- Fig. S10** EDS element mapping images of the cross section of freeze-dried PCMH@TPE microtube
- Fig. S11** Peeling test curve of PCMH@TPE microtube
- Fig. S12** Stress-strain curves of PNIPAM/clay hydrogel and PCMH
- Fig. S13** Cyclic tensile loading-unloading curves of PCMH@TPE microtube at a fixed maximum strain of 1000%
- Fig. S14** NIR-induced volume shrinkage of PCMH with  $0.8 \text{ mg mL}^{-1}$  MXene
- Fig. S15** Vis-NIR spectra of MXene aqueous dispersion before and after NIR laser irradiation for 30 min and 90 min
- Fig. S16** Changes of TPE outer diameter, PCMH wall thickness, and corresponding channel size of PCMH@TPE microtube at a fixed strain of 100% in ten heating-cooling cycles
- Fig. S17** Channel size changes of PCMH@TPE microtube upon NIR irradiation and cooling at  $4 \text{ }^\circ\text{C}$
- Fig. S18** Changes of TPE outer diameter, PCMH wall thickness, and corresponding channel size of PCMH@TPE microtube in ten NIR irradiation-cooling cycles
- Fig. S19** Schematic design for real-time monitoring the differential pressure of PCMH@TPE microtube
- Fig. S20** Tensile strain-dependent changes of PCMH@TPE microtube channel size, PCMH wall thickness and TPE outer diameter
- Fig. S21** Cyclic flow pressure changes at the inlet and outlet of PCMH@TPE microtube-based strain sensor
- Fig. S22** Differential pressure changes of PE tube by switching water flow between  $4 \text{ }^\circ\text{C}$  and  $40 \text{ }^\circ\text{C}$
- Fig. S23** Comparison of the tensile strength, elongation-at-break and Young's moduli of the reported tubular structures with different materials

#### **References S1-S19**

**Movie S1.** PCMH@TPE microtube serves as temperature and NIR-driven valve in liquid control

## Experimental

**Materials.** *N*-Isopropylacrylamide (NIPAM) was obtained from J&K Chemical Co. Ltd. Clay nanosheet, laponite XLG ( $[\text{Mg}_{5.34}\text{Li}_{0.66}\text{Si}_8\text{O}_{20}(\text{OH})_4]\text{Na}_{0.66}$ ), was obtained from Anwu Technology Co., Ltd. (Beijing, China). Thermoplastic elastomer (TPE, styrene-isoprene-styrene block copolymer, styrene 22 wt%), potassium persulfate (KPS), and *N,N,N',N'*-tetramethylethylenediamine (TEMED) were purchased from Sigma-Aldrich. Titanium aluminum carbide ( $\text{Ti}_3\text{AlC}_2$ ) was purchased from 11 Technology Co., Ltd. (Jilin, China). 4-Acryloylbenzophenone (4-ABP) was synthesized according to literature.<sup>S1</sup> Hydrochloric acid (HCl) and dichloromethane (DCM) was purchased from Sinopharm Chemical Reagent Co., Ltd. Lithium fluoride (LiF), rhodamine B, and methylene blue were obtained from Macklin Chemical Co. Ltd. Except that NIPAM was recrystallized prior to use, other reagents were not further purified.

**Synthesis of MXene ( $\text{Ti}_3\text{C}_2\text{T}_x$ ).** The preparation of delaminated MXene nanosheets was the same as previously reported.<sup>S2</sup> Briefly, 2 g of LiF was added to 40 mL of 9 M HCl aqueous solution in a polypropylene container, and after stirring for 5 min, 1.98 g of  $\text{Ti}_3\text{AlC}_2$  powder was slowly added to the mixture solution in 5 min in an ice water bath. The mixture reacted for 24 h in an oil bath at 35 °C. Deionized water was then added to the obtained mixture followed by centrifugation at 3500 rpm for 5 min several times until the pH of the supernatant was >6. A dark blue precipitate was obtained, which was re-dispersed in deionized water, and ultrasonicated for one hour in an ice water bath under nitrogen protection. After centrifuging at 3500 rpm for 1 h, the delaminated  $\text{Ti}_3\text{C}_2\text{T}_x$  supernatant was obtained, which was further freeze-dried for 48 h to obtain  $\text{Ti}_3\text{C}_2\text{T}_x$  solids for storage.

**Preparation of PNIPAM/clay/MXene hydrogels (PCMH) in glass tube.** First, 0.13 g of clay nanosheets was added to 4.4 mL of deionized water (according to the total volume) and stirred overnight to obtain a clear dispersion. Then, 0.5 g of the NIPAM monomer was added to the dispersion and stirred until being completely dissolved. Afterwards, a certain amount of 10 mg mL<sup>-1</sup> MXene dispersion was added to the monomer solution, and sonicated for 10 min in an ice water bath. This final solution was purged with nitrogen in an ice water bath for more than 3 h to remove dissolved oxygen. Thereafter, 4 μL of TEMED and 200 μL of 2.5 wt% KPS aqueous solution as the polymerization accelerator and initiator respectively, were added to the solution. The mixed solution was centrifuged at 2200 rpm for 10 s to remove air bubbles, then injected into a glass tube with an inner diameter of 1.6 mm, and reacted at 4 °C for 12 h to obtain the composite hydrogel. The hydrogels with different concentrations of MXene (0, 0.2, 0.4, 0.8, 1.2, and 1.6 mg mL<sup>-1</sup>) were synthesized by adding 0, 100, 200, 400, 600 and 800 μL of 10 mg mL<sup>-1</sup> MXene aqueous dispersion respectively, and the total volume of precursor solution was kept at 5 mL by adjusting the amount of added deionized

water.

**Preparation of TPE microtube.** TPE tubes with different shapes and sizes of cross-sections were prepared under same conditions by a modified evaporation-induced deposition method<sup>S3,4</sup>, as shown in Figure S1. In brief, for a typical round-shaped TPE tube, 20 wt% TPE solution in dichloromethane was injected into a glass tube with an inner diameter of 1.6 mm, and then dried in an oven at 50 °C. When necessary, the glass tube can be removed by diamond cutting in the middle and pulling out or direct HF dissolution. It should be noted that the presence of bubbles in the solution should be avoided to form a smooth tube. Changing the shapes of glass tubes does not significantly influence the deposition process and tube quality.

**Preparation of PCMH@TPE microtube.** As shown in Figure S1, 10 wt% 4-ABP in ethanol was first injected into the as-prepared TPE microtube adhered on the inner wall of glass tube (inner diameter ~ 1.6 mm) for 20 min. Then the tube was washed three times with methanol and deionized water, and dried with nitrogen. After that, a paraffin-coated capillary (outer diameter ~ 0.9 mm) was inserted into the tube with coaxial assembly and fixed with stainless steel needles. The PCMH pre-gel solution was injected into the gap between TPE tube and capillary, follow by UV light irradiation for 1 h at 0 °C to initiate polymerization and interfacial bonding between hydrogel and elastomer. The whole device was placed at 4 °C for another 12 h to allow the hydrogel to completely polymerize. Afterwards, the capillary was carefully removed, and the shell glass tube can be removed by diamond cutting method. The resulting PCMH@TPE microtube was further swollen for several days in water at 4 °C for subsequent uses.

**Fabrication of PCMH@TPE microfluidic valve.** For the PCMH@TPE microfluidic valve, the capillary with an outer diameter of 0.4 mm and shell glass tube with an inner diameter of 1.6 mm was used. Before use, the PCMH@TPE microfluidic valve was swollen at 4 °C for 2 h until the channel was completely closed.

**Characterizations.** Differential scanning calorimetry (DSC250, TA) of PCMH was performed under N<sub>2</sub> atmosphere at a temperature ramp of 10 °C min<sup>-1</sup> from 20 to 45 °C. Scanning electron microscopy (SEM) and energy dispersive X-ray spectroscopy (EDS) images were taken on a Quanta 250 microscope at 12.5 kV. Transmission electron microscopy (TEM) images of MXene nanosheets were acquired on JEM-2100. Atomic force microscope (AFM) images and height profiles were recorded on Bruker Multimode 8. The vis-NIR spectra of MXene aqueous solutions were collected on a spectrophotometer (PerkinElmer, Lambda 950). ATR-FTIR spectra were recorded on a Nicolet iS50 (Thermo Scientific) spectrometer with diamond crystal as the window material. X-ray diffraction (XRD)

was performed on Bruker D8 diffractometer (Germany) with Ni-filtered Cu K $\alpha$  radiation at 40 kV and 40 mA. The images of the cross-sections of PCMH@TPE microtubes were taken on an Olympus SZX7 microscope. Mechanical properties of PCMH@TPE microtubes were evaluated by a universal testing machine (Suns, TUM 2103). PCMH@TPE microtube samples for mechanical tests have a size of 1.5 cm in length, 1.6 mm in outer diameter and 320  $\mu$ m in channel size at 25  $^{\circ}$ C.

**Swelling-shrinking curves of PCMH@TPE microtube.** In the case of temperature-responsive swelling-shrinking, the temperature was controlled by a Linkam hot stage with a scanning rate of 4.1  $^{\circ}$ C min $^{-1}$ , and kept at 45  $^{\circ}$ C for 3 min. The channel size changes were monitored by an optical microscope per 30 s in the early stage of heating and cooling process, per 10 min in the first hour of swelling at 4  $^{\circ}$ C, and per 1 h in the rest swelling process. In the case of swelling-shrinking at a fixed strain of 100%, the two ends of microtube were fixed on a vernier caliper, heated at 45  $^{\circ}$ C for 3 min in an oven and then swollen in a refrigerator at 4  $^{\circ}$ C for 2 h. In the case of NIR-responsiveness, a cross-sectional sample of the microtube was fixed in a sample tray with about 50  $\mu$ L of water, and irradiated with NIR light with the power density of 1.5 W cm $^{-2}$  for 2 min and then cooled at 4  $^{\circ}$ C for swelling.

**Strain sensing of the flow pressure of PCMH@TPE microtube.** A continuous fluid ( $Q = 300 \mu$ L min $^{-1}$ ) was supplied for PCMH@TPE microtube using a syringe pump. The microtube channels were connected to PE pipes with stainless tubes. Two pressure gauges (PS3, MesoBioSys Co., Ltd.) were connected near the inlet and outlet of PCMH@TPE microtube for real-time monitoring flow pressure changes (schematic design in Figure S14). Continuous cyclic loading and unloading processes under different strains were performed on a universal testing machine. PCMH@TPE microtube sample for strain sensing has a length of 3.5 cm, diameter of 1.6 mm, and channel size of 320  $\mu$ m at room temperature. The strain sensing of PCMH@TPE microtube with flattened wrinkles was monitored by continuously injecting water at 45  $^{\circ}$ C.

**Compression sensing of the flow pressure of PCMH@TPE microtube.** A continuous fluid ( $Q = 300 \mu$ L min $^{-1}$ ) was supplied for PCMH@TPE microtube. The PCMH@TPE microtube was fixed on the substrate of a mechanical tester (ESM303, MARK-10) and a gauge sensor with a range of 1 N was used to apply different forces (0.1, 0.2, ..., 0.8 N) to the middle of the tube by an indenter with a diameter of 1 cm at 13 mm min $^{-1}$  compression speed.

**Temperature and NIR light sensing of the flow pressure of PCMH@TPE microtube.** For temperature sensing, the water flow with a flow rate of 200  $\mu$ L min $^{-1}$  was pre-heated/cooled by a hot plate, switching between 4 and 40  $^{\circ}$ C. For NIR light sensing, a water flow of 4  $^{\circ}$ C continuously flows into the tube at the same flow rate of 200  $\mu$ L min $^{-1}$ . The NIR laser was intermittently exposed to the

inlet end of PCMH@TPE microtube with a power density of  $1.5 \text{ W cm}^{-2}$ .

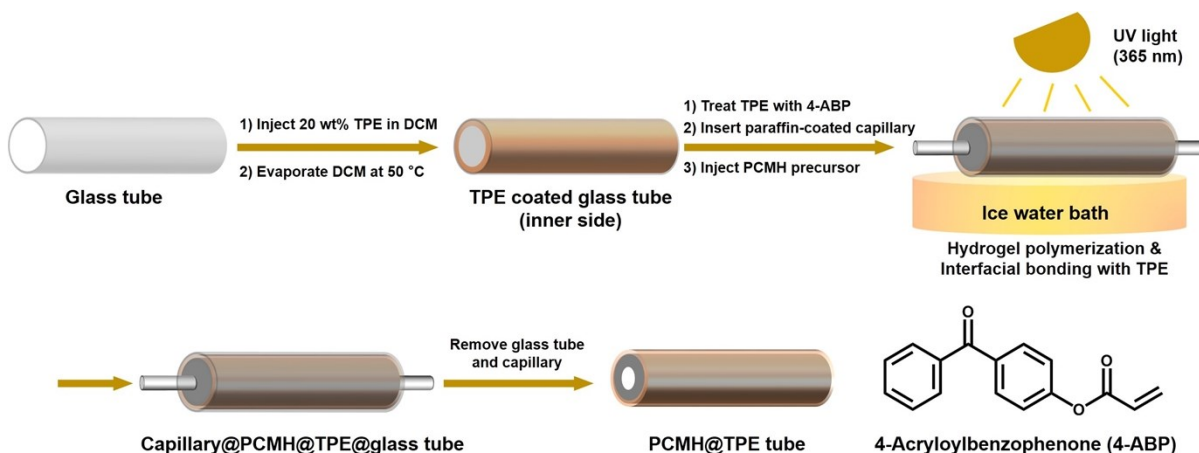


**Fig. S1 Schematic fabrication process of PCMH@TPE microtube.** DCM = dichloromethane. See detailed descriptions in the experimental section.

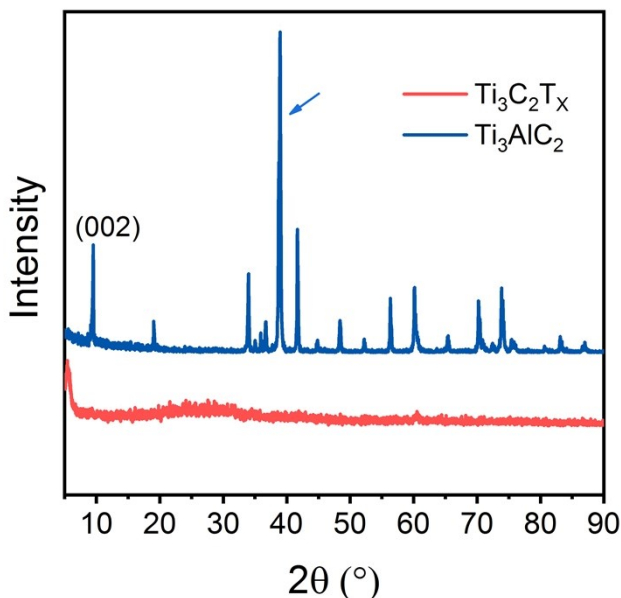


**Fig. S2 XRD profiles of raw  $\text{Ti}_3\text{AlC}_2$  and exfoliated 2D MXene ( $\text{Ti}_3\text{C}_2\text{T}_x$ ) nanosheets.** That the (002) peak downshifts to a lower angle and the typical intense diffraction peak of  $\text{Ti}_3\text{AlC}_2$  at  $2\theta \approx 39^\circ$  disappears demonstrates that  $\text{Ti}_3\text{AlC}_2$  MAX phase has been successfully exfoliated and MXene nanosheets were obtained<sup>S5, 6</sup>.

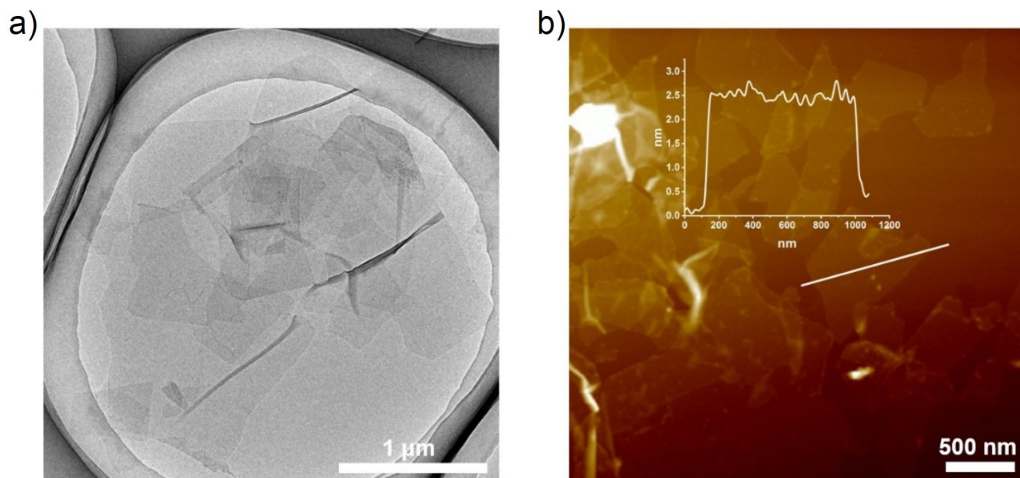


**Fig. S3 Typical (a) TEM and (b) AFM images of MXene nanosheets demonstrate its ultra-thin monolayer feature with a planar size of 0.5-2  $\mu\text{m}$  and a height of approximately 2 nm.**

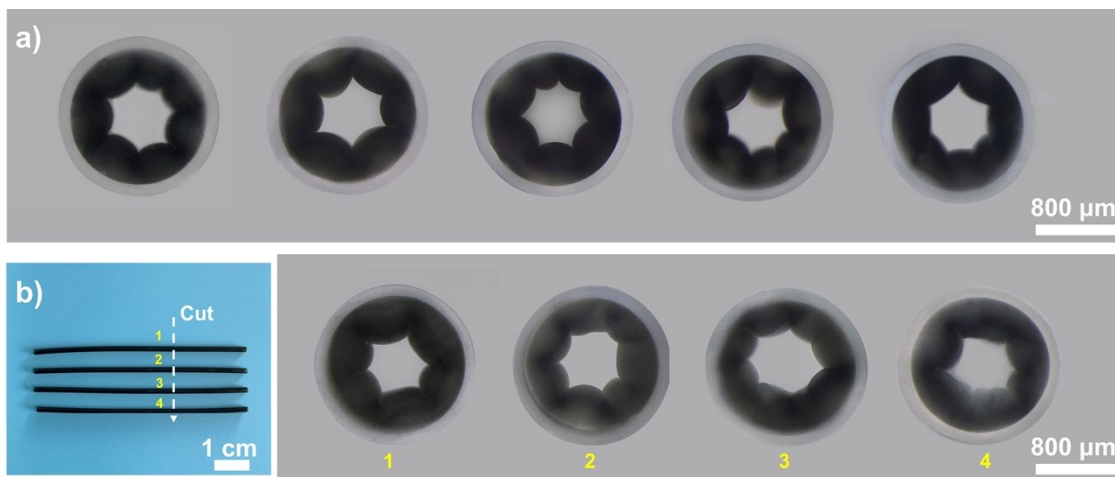


**Fig. S4 a) Cross-sectional images of a single PCMH@TPE microtube at different positions and b) multiple cross-sectional images of four different tubes.**

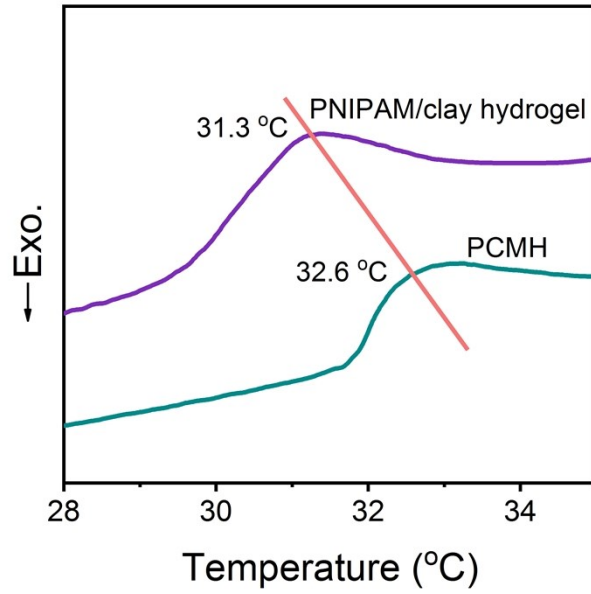


**Fig. S5** DSC heating curves of PNIPAM/clay hydrogel and PCMH with 0.8 mg mL<sup>-1</sup> MXene (scanning rate: 10 °C min<sup>-1</sup>). The VPTTs of the two hydrogels are also labelled.

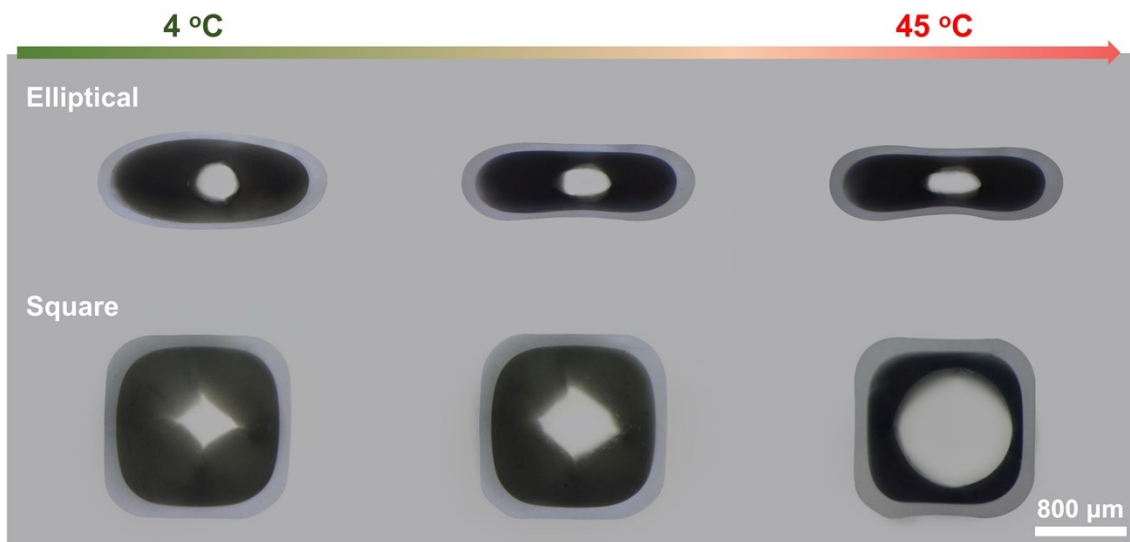


**Fig. S6** Heat-induced channel size changes of PCMH@TPE microtubes with elliptical and square cross-sections.

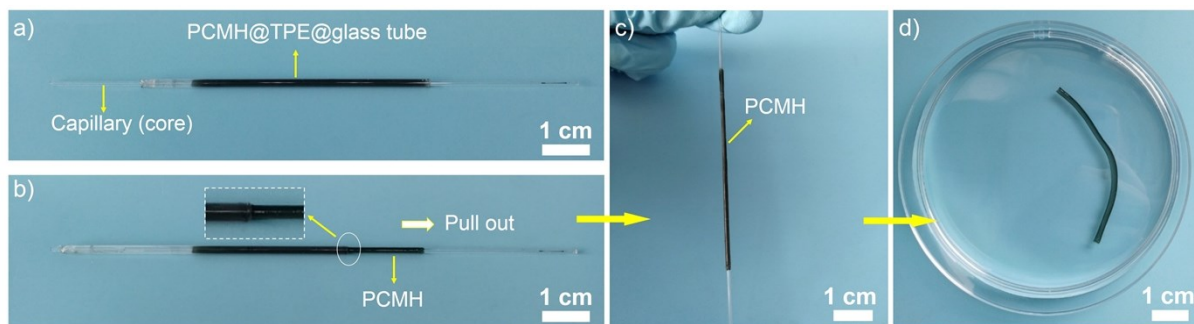


**Fig. S7 Optical images of PCMH peeled from TPE tube pre-treated with benzophenone.** a, b) PCMH is easily extracted from the TPE tube. c, d) The paraffin-coated capillary in the hydrogel tube can be removed without difficulty when immersed in deionized water.

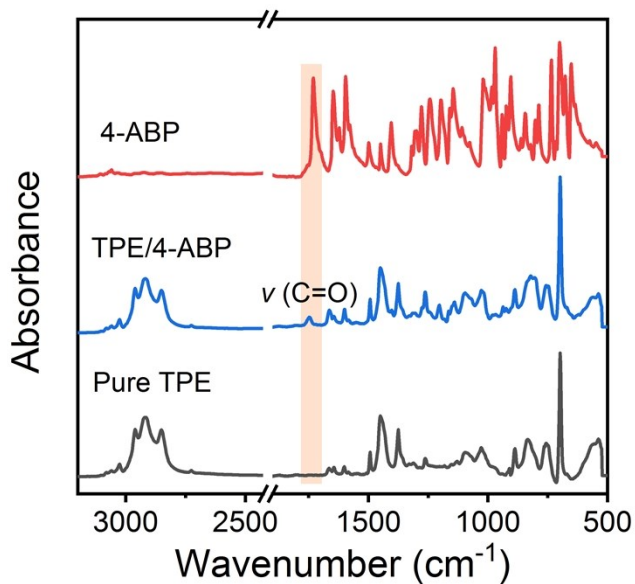


**Fig. S8 ATR-FTIR spectra of 4-ABP, 4-ABP treated TPE and pure TPE.** The stretching band of carbonyl group at  $1745 \text{ cm}^{-1}$  comes from 4-ABP.

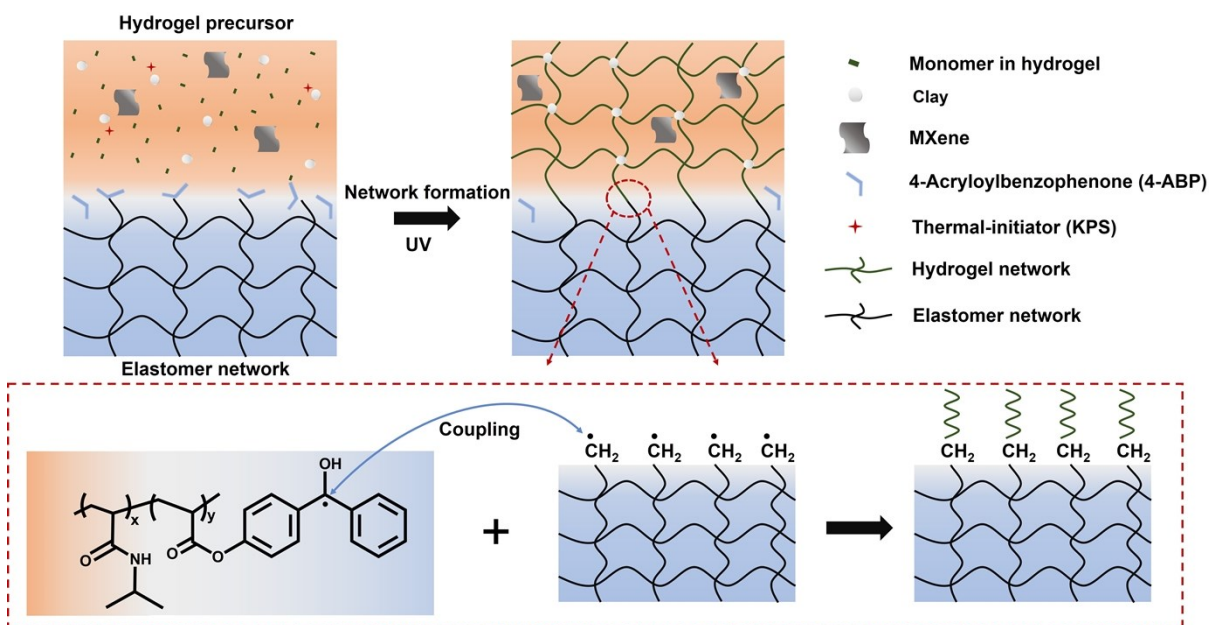


**Fig. S9 Schematic interfacial bonding between PCMH and TPE with the strategy of 4-ABP pre-treatment.** Under the action of thermal initiator (KPS) and UV light, the double bond of 4-ABP absorbed on the surface of TPE could copolymerize with NIPAM. Meanwhile, the benzophenone group of 4-ABP can extract hydrogen atoms from the C-H groups of elastomer to form a free radical, which then couples with the benzophenone ketyl group, forming strong interfacial bonds between PCMH and TPE.

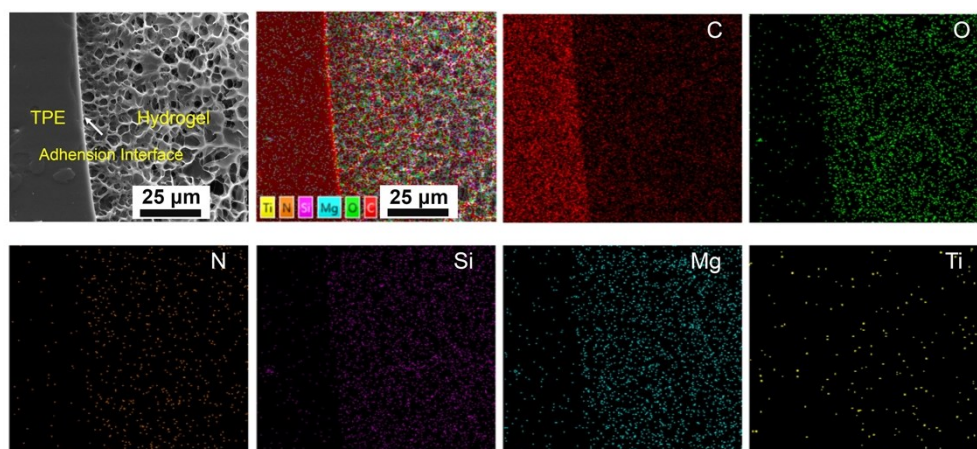


**Fig. S10 EDS element mapping images of C, O, N, Si, Mg, Ti of the cross section of freeze-dried PCMH@TPE microtube.**

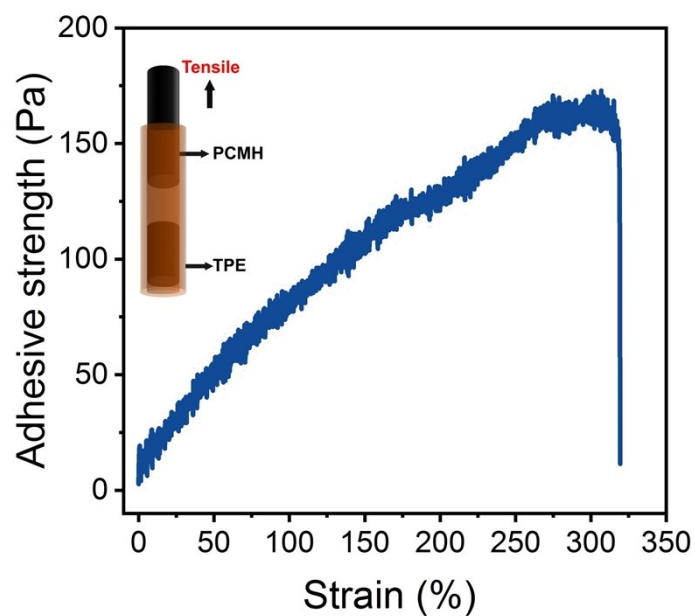


**Fig. S11 Peeling test curve of PCMH@TPE microtube.** For sample preparation, as the TPE@glass tube was treated with 4-ABP, another empty glass tube with an outer diameter of 1.3 mm was attached to TPE@glass tube. Then, a pre-gel solution of PCMH was injected into the two tubes and polymerized upon UV illumination with a small gap in the middle of TPE tube. The adhesive strength was calculated by dividing the tensile force by the contact area between adhered hydrogel and TPE.

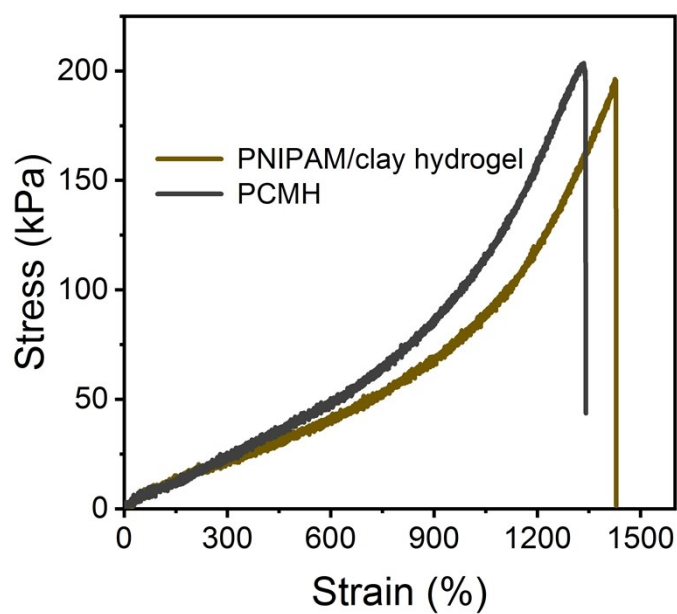


**Fig. S12 Stress-strain curves of PNIPAM/clay hydrogel and PCMH with a tensile speed of 100 mm min<sup>-1</sup>.**

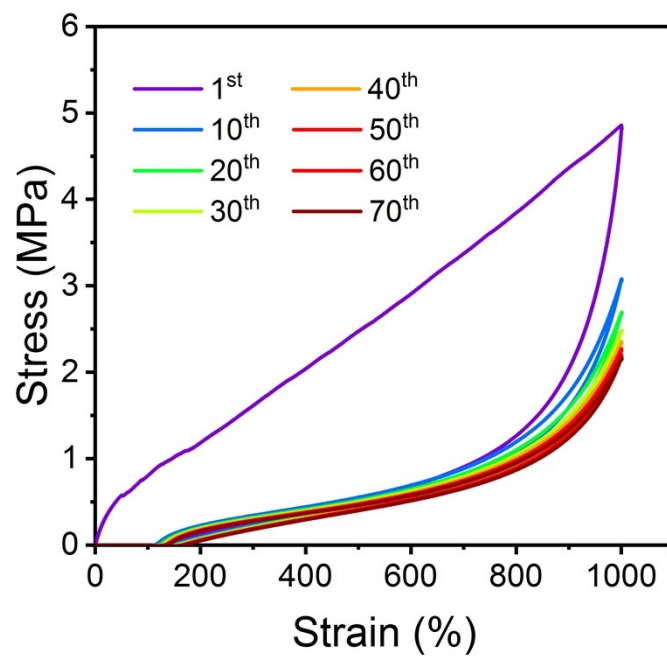


**Fig. S13** Cyclic tensile loading-unloading curves of PCMH@TPE microtube at a fixed maximum strain of 1000% with a tensile speed of 100 mm min<sup>-1</sup>.

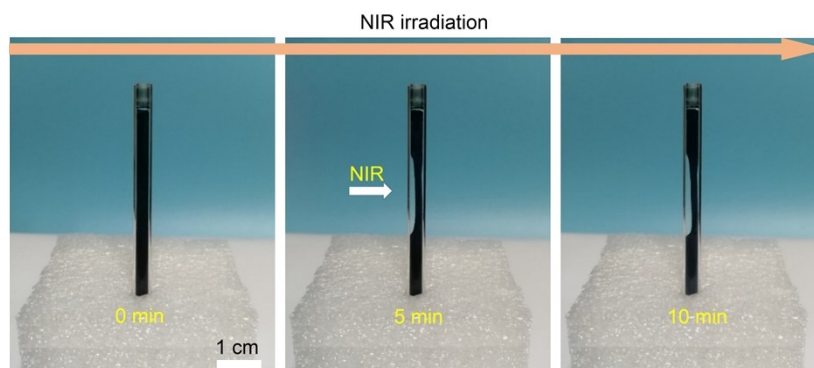


**Fig. S14** NIR-induced volume shrinkage of PCMH with 0.8 mg mL<sup>-1</sup> MXene. The power density of NIR illumination is 1.5 W cm<sup>-2</sup>.

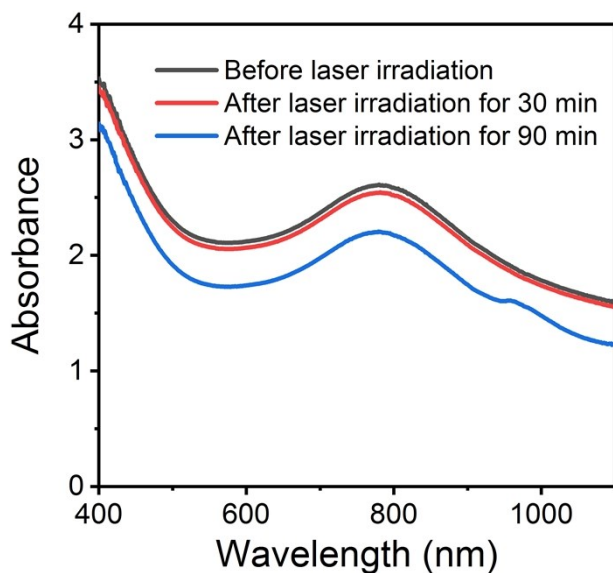


Fig. S15 Vis-NIR spectra of MXene aqueous dispersion (0.1 mg mL<sup>-1</sup>) before and after NIR laser irradiation for 30 min and 90 min.

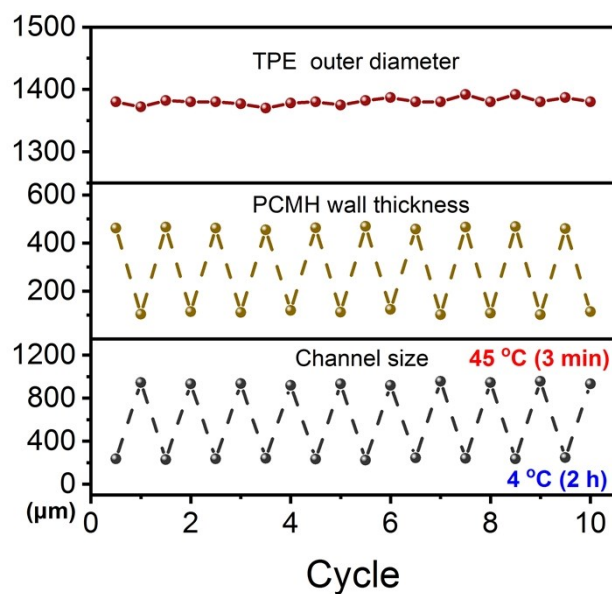


Fig. S16 Changes of TPE outer diameter, PCMH wall thickness, and corresponding channel size of PCMH@TPE microtube at a fixed strain of 100% in ten heating-cooling cycles.

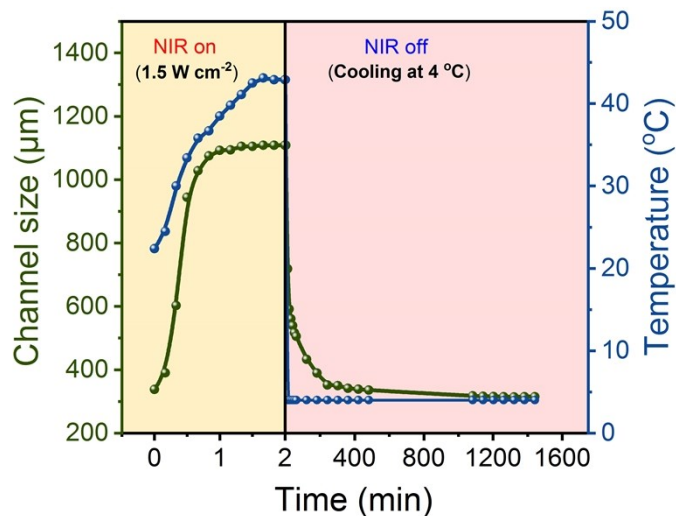


Fig. S17 Channel size changes of PCMH@TPE microtube upon NIR irradiation with the power density of  $1.5 \text{ W cm}^{-2}$  (starting from room temperature) and then cooling at  $4 \text{ }^\circ\text{C}$ .

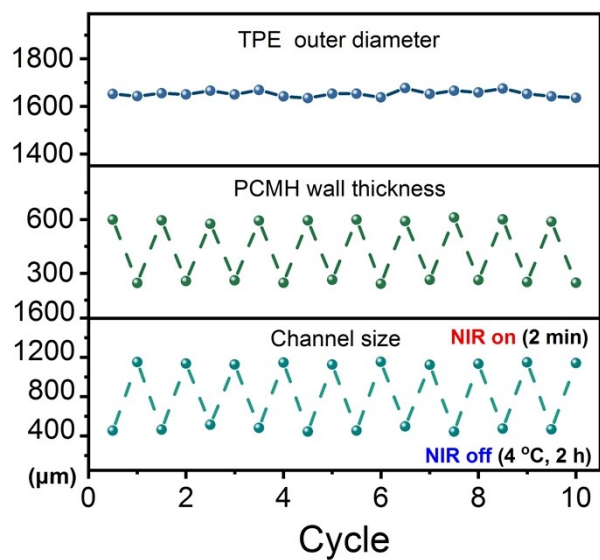


Fig. S18 Changes of TPE outer diameter, PCMH wall thickness, and corresponding channel size of PCMH@TPE microtube in ten NIR irradiation-cooling cycles.

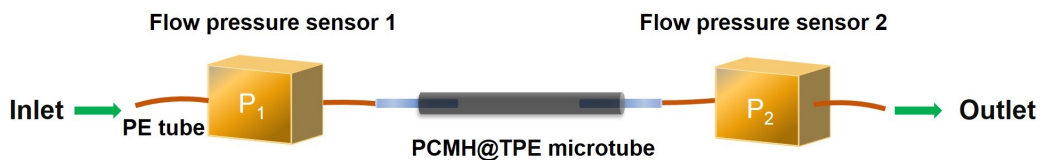


Fig. S19 Schematic design for real-time monitoring the differential pressure of PCMH@TPE microtube. The differential pressure,  $\Delta P = P_1 - P_2$ .

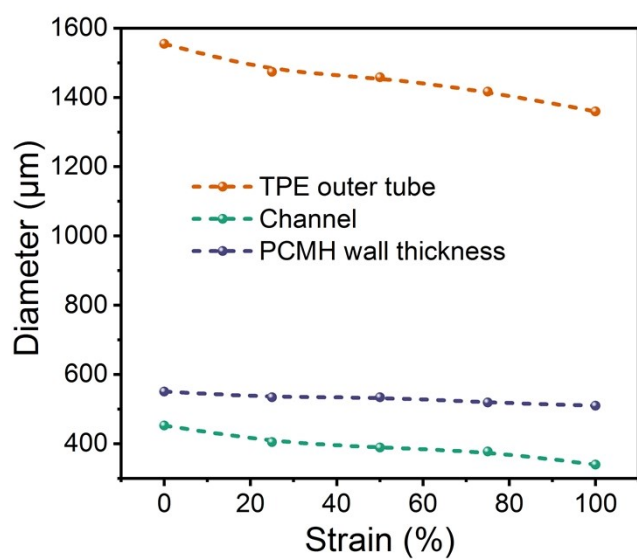


Fig. S20 Tensile strain-dependent changes of PCMH@TPE microtube channel size, PCMH wall thickness and TPE outer diameter.

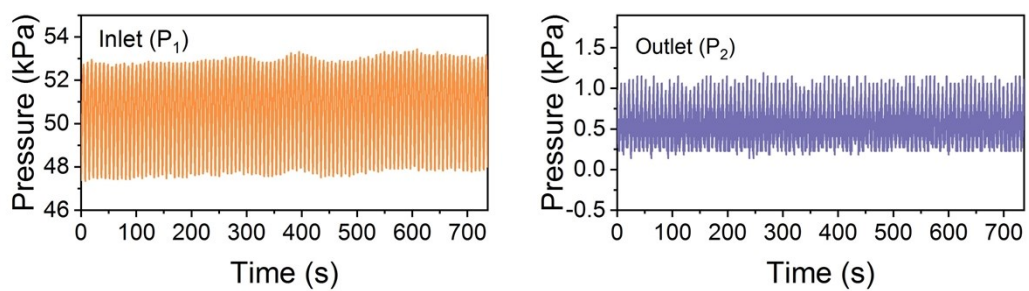


Fig. S21 Cyclic flow pressure changes at the inlet (P<sub>1</sub>) and outlet (P<sub>2</sub>) of PCMH@TPE microtube-based strain sensor under 50% strain for 100 cycles.

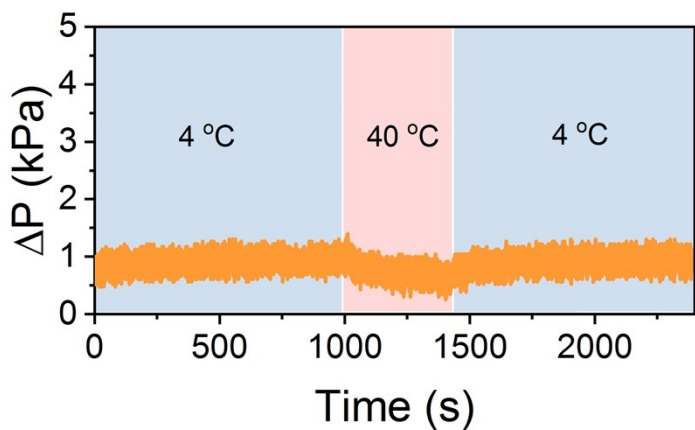


Fig. S22 Differential pressure changes of PE tube by switching water flow between 4 °C and 40 °C showing no significant temperature response.

**Table S1. Comparison of the tensile strength, elongation-at-break and Young's moduli of the reported tubular structures with different materials.** The PCMH@TPE microtube with a hybrid elastomer-hydrogel structure shows superior or comparable mechanical toughness to most of the reported tubular materials.

Tubular systems		Tensile strength (MPa)	Elongation at break (%)	Young's modulus (MPa)	Ref.
Healthy human coronary artery		1.44 ± 0.87	54 ± 25	1.55 ± 0.26	S7
Hydrogel-elastomer hybrid tubes	PCMH@TPE	5.6	1100	1.3	This work
	SBS-coated Cu-alginate	~0.019	~16	~0.26	S8
	Silk/PAAm/TPU	3.11±0.93	95 ± 22	1.44 ± 0.29	S9
Tubular plastics	PCL	7.7±2.5	210.8 ± 70.9	10.6 ± 4.2	S10
	PLGA	3.0±0.4	19.7 ± 8.8	78.9 ± 19.8	
	PCL-PLGA	3.5±1.9	138.7 ± 25.2	79.2 ± 43.8	
Tubular hydrogels	PDGI/PAAm	0.028~0.092	200~1100	-	S11
	SA/AAm/heparin	0.045	~560	-	S12
	PAAm/PAA-Fe	0.1~2.5	130~270	0.1~1.7	S13
	PAA-co-AAm-C18/Fe <sup>3+</sup>	~0.19	~210	0.01-0.08	S14
	Ca-alginate	0.036	~70	0.05	S15
	Cu-alginate	~0.014	-	-	S8
	PNIPAM-PAA/PAAm-PAA/Fe <sup>3+</sup> (ABA type)	0.14	155	~0.09	S16
	Necklace-like Cu-alginate	0.07~0.25	11~23	-	S17
	Gelatin	0.045~0.09	13~25	0.33~0.73	S18
Microchannels in elastomer matrix	PDMS	6.3	368±31	-	S19
	VHB	1.1	967±40	0.06	

## References

- S1. G. Stoychev, N. Pureskiy and L. Ionov, *Soft Matter*, 2011, **7**, 3277-3279.
- S2. M. R. Lukatskaya, S. Kota, Z. Lin, M.-Q. Zhao, N. Shpigel, M. D. Levi, J. Halim, P.-L. Taberna, M. W. Barsoum, P. Simon and Y. Gogotsi, *Nat. Energy*, 2017, **2**, 17105.
- S3. J.-a. Lv, Y. Liu, J. Wei, E. Chen, L. Qin and Y. Yu, *Nature*, 2016, **537**, 179.
- S4. B. Xu, C. Zhu, L. Qin, J. Wei and Y. Yu, *Small*, 2019, **15**, 1901847.
- S5. L. Ding, Y. Wei, Y. Wang, H. Chen, J. Caro and H. Wang, *Angew. Chem. Int. Ed.*, 2017, **56**, 1825-1829.

- S6. R. Han and P. Wu, *J. Mater. Chem. A*, 2019, **7**, 6475-6481.
- S7. A. Karimi, M. Navidbakhsh, A. Shojaei and S. Faghihi, *Mater. Sci. Eng., C*, 2013, **33**, 2550-2554.
- S8. Q. Chen, S. Liang, X. Song, P. Naumov and L. Zhang, *Chem. Commun.*, 2018, **54**, 10304-10307.
- S9. H.-Y. Mi, Y. Jiang, X. Jing, E. Enriquez, H. Li, Q. Li and L.-S. Turng, *Mater. Sci. Eng., C*, 2019, **98**, 241-249.
- S10. S. Cheng, Y. Jin, N. Wang, F. Cao, W. Zhang, W. Bai, W. Zheng and X. Jiang, *Adv. Mater.*, 2017, **29**, 1700171.
- S11. Y. Wang, W. Niu, C.-Y. Lo, Y. Zhao, X. He, G. Zhang, S. Wu, B. Ju and S. Zhang, *Adv. Funct. Mater.* 2020, **30**, 2000356.
- S12. J. Deng, C. Cheng, Y. Teng, C. Nie and C. Zhao, *Polym. Chem.*, 2017, **8**, 2266-2275.
- S13. S. Ma, M. Rong, P. Lin, M. Bao, J. Xie, X. Wang, W. T. S. Huck, F. Zhou and W. Liu, *Chem. Mater.*, 2018, **30**, 6756-6768.
- S14. L. Han, Y. Zheng, H. Luo, J. Feng, R. Engstler, L. Xue, G. Jing, X. Deng, A. del Campo and J. Cui, *Angew. Chem. Int. Ed.*, 2020, **59**, 5611-5615.
- S15. L. Ouyang, J. A. Burdick and W. Sun, *ACS Appl. Mater. Interfaces*, 2018, **10**, 12424-12430.
- S16. H. Lin, S. Ma, B. Yu, M. Cai, Z. Zheng, F. Zhou and W. Liu, *Chem. Mater.*, 2019, **31**, 4469-4478.
- S17. S. Liang, Y. Tu, Q. Chen, W. Jia, W. Wang and L. Zhang, *Mater. Horiz.*, 2019, **6**, 2135-2142.
- S18. L. Zhang, Y. Xiang, H. Zhang, L. Cheng, X. Mao, N. An, L. Zhang, J. Zhou, L. Deng, Y. Zhang, X. Sun, H. A. Santos and W. Cui, *Adv. Sci.* 2020, **7**, 1903553.
- S19. F. Wu, S. Chen, B. Chen, M. Wang, L. Min, J. Alvarenga, J. Ju, A. Khademhosseini, Y. Yao, Y. S. Zhang, J. Aizenberg and X. Hou, *Small*, 2018, **14**, 1702170.